Theor Chem Account (2008) 121:155–164
DOI 10.1007/s00214-008-0458-z

REGULAR ARTICLE

Theoretical studies of the spectroscopic properties of blue emitting iridium complexes

Tao Liu · Bao-Hui Xia · Xin Zhou · Qing-Chuan Zheng · Qing-Jiang Pan · Hong-Xing Zhang

Received: 11 March 2008 / Accepted: 20 May 2008 / Published online: 11 June 2008

Abstract Electronic structures, absorptions and emissions of a series of $(ppy)_2Ir(acac)$ derivatives (ppy = 2-phenylpyridine; acac = acetoylacetonate) with fluoro substituent on ppy ligands were investigated theoretically. The ground and excited states geometries were fully optimized at B3LYP/LANL2DZ and CIS/LANL2DZ level, respectively. The HOMO is composed of d(Ir) and π (C^N), while the LUMO is localized on C^N ligand. The absorptions and emissions in CH_2Cl_2 media were calculated under the TD–DFT level with PCM model. The lowest-lying absorption of these complexes is dominantly attributed to metal-to-ligand and intraligand charge transfer (MLCT/ILCT) transitions and the emission of them originates from ^{3}MLCT/^{3}ILCT excited states. The absorption and emission of these complexes are blue-shifted by increasing the number of fluoro on phenyl, but the spectra are red-shifted by adding fluoro on pyridyl. While a single fluoro of different substituted site on phenyl results in different extent blue-shift to the spectra.

Keywords Iridium complexes · Phosphorescence · DFT

Electronic supplementary material The online version of this article (doi:10.1007/s00214-008-0458-z) contains supplementary material, which is available to authorized users.

T. Liu · B.-H. Xia · X. Zhou · Q.-C. Zheng · Q.-J. Pan · H.-X. Zhang (✉)
State Key Laboratory of Theoretical and Computational Chemistry, Institute of Theoretical Chemistry, Jilin University, Changchun 130023, People's Republic of China
e-mail: zhanghx@mail.jlu.edu.cn

T. Liu
e-mail: liutao@email.jlu.edu.cn

B.-H. Xia
College of Chemistry, Jilin University, Changchun 130023, People's Republic of China

Q.-J. Pan
Laboratory of Physical Chemistry, School of Chemistry and Materials Science, Heilongjiang University, Harbin 150080, People's Republic of China

1 Introduction

Since it was reported that organic light-emitting devices (OLEDs) prepared with tris–cyclometalated complexes such as fac-[Ir(ppy)$_3$](ppy$^-$ = 2-phenylpyridine) have efficiencies greater than 80%, Ir(III) complexes have attracted considerable much attention [1–10].

The Ir(III) phosphorescent materials, such as Ir(C^N)$_2$L(C^N = ppy, bzq, btp, thp, bt etc.; L = acac, dbm, tmd, bza etc.), have been synthesized and their spectroscopic properties have been investigated experimentally and theoretically by Thompson and Hay [1–4,11]. These complexes exhibit both MLCT and $\pi\pi^*$ absorptions in nature, while their phosphorescence originate from ^{3}MLCT/^{3}ILCT excited states. The OLEDs based on $(ppy)_2Ir(acac)$, $(bt)_2Ir(acac)$ and $(btp)_2Ir(acac)$ give green, yellow, and red phosphorescent color, respectively [1–4].

However, the most interesting and challenging color remains the blue color, because the efficient "deep blue" light emitters represent the most important component for fabricating the white light emitting devices (WOLEDs) [12–17]. At present, the studies of the blue luminescent material on experiment and theory mainly have been focused on aromatic organic molecules or conjugated organic polymers such as poly(p-phenylene), polyfluorenes, polycarbazoles, polythiophene derivatives, derivatives of poly-paraphenylene with ladder structures, and some copolymers based on fluorine or pyridine. Furthermore, these blue emitting materials have been introduced as the emitter in OLED device [18–23].

Due to the absence of the spin-orbital coupling effects, the emissions of these polymers are dominated by fluorescence. But it is well-known that the phosphorescent emissions are of considerable importance because they can increase the luminescent life-time and quantum yields effectively. Therefore, it is very promising to seek the suitable blue phosphorescent materials. One effective way of promoting phosphorescent emission from organic molecules is to import d-block metal centers into the organic systems.

Blue phosphorescent materials based on inorganic semiconductors are well-known [2,24–26], but the inorganic and organometallic complexes suitable for blue phosphorescent materials are rather rare and have been limited to 8-hydroxyquinoline-, 7-azaindole-, or azomethine-based complexes where either Al(III), B(III), or Zn(II) ion is involved [25,27–29]. For example, Che and co-workers [30, 31] have reported a Zn(II) complexes $Zn_4O(7\text{-azaindolyl})_6$, which emits a blue color at 433 nm in the solid state. Wang and co-workers [32,33] have found that a series of Al(III) complexes emitting between 420 and 450 nm were suitable for blue luminescent materials.

Recently, several blue phosphorescent Ir(III) complexes such as fac-Ir(flz)$_3$ (flz = (9,9-dimethyl-2-fluorenyl) pyrazolyl), ($F_n$ppy)$_2$ Ir(acac) (n = 3: F_3ppy = 2-(3′, 4′, 6′-trifluorophenyl)pyridine; n = 4: F_4ppy = 2-(3′, 4′, 5′, 6′-tetrafluorophenyl)pyridine) and (X-ppz)$_2$Ir(N^N)$^+$(X = 4′, 6′-difluoro; N^N = 4,4-di- tert-butyl-2,2′-bipyridine) have been investigated by Thompson [2,34] and Naso et al. [35,36], moreover, $(C_4H_9)_4$N[Ir(2-(2,4-difluorophenyl) -pyridine)$_2$(CN)$_2$], $(C_4H_9)_4$N[Ir-(2-(2,4-difluorophenyl)-4- dimethylaminopyridine)$_2$(CN)$_2$], and $(C_4H_9)_4$N[Ir(2-(3,5-difluorophenyl) -4-dimethylaminopyridine)2-(CN)$_2$], and [Ir(2,4-difluorophenylpyridine)2(4,4′-dimethylamino-2,2′-bipyridine)](PF$_6$) (N969) were investigated by De Angelis et al. [37,38] experimentally, and the phosphorescence of these complexes localizing between 450 and 500 nm originate from ^{3}MLCT excited state. Furthermore, Hong and co-workers [39] have found that fine color tuning of complexes (ppy)$_2$Ir(acac) substituted by methyl group could be achieved by varying the sites of electron-donating methyl substituent on the phenylpyrazole. The iridium complexes carrying fluorinated phenylpyridyl ligands have shown several benefits, such as enhancing the photoluminescence efficiency and improving the sublimation [40,41], which stimulates us to investigate the optical mechanism. Especially, it is more practical to investigate the influence of the substituents to the spectral properties.

Herein, based on the above background, we performed theoretical calculation on a series of (ppy)$_2$Ir(acac) derivatives **1**–**12** (see Fig. 1) using ab initio and density functional theory [42] (DFT) methods. Complex **1** is (ppy)$_2$Ir(acac), complexes **2**–**5** are (ppy)$_2$Ir(acac) derivatives with 1, 2, 3 and 4 fluoro groups substituted on phenyl, complexes **6**–**8** are (ppy)$_2$Ir(acac) derivatives with one fluoro group substituted

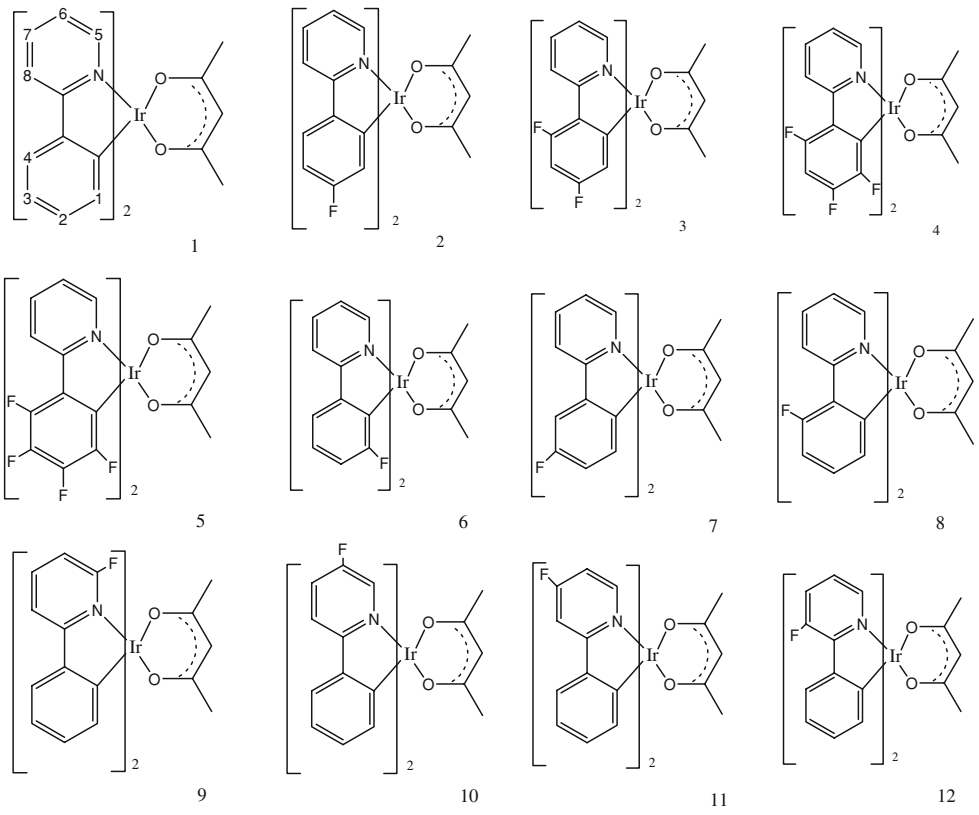

Fig. 1 Sketch structures of computational complexes **1**–**12**

on phenyl with different sites, and **9**–**12** are $(ppy)_2Ir(acac)$ derivatives with one fluoro group substituted on pyridyl with different sites. The ground and excited states geometries, the properties of the frontier molecular orbitals (FMOs), and the electronic absorptions as well as the emissions have been explored. Highly important, the relationships between the electronic structures and the optical properties have been explored. The significant influence of the fluoro substituent on C^N ligand rationalizes the tunable optical properties of the complexes.

2 Computational details

C_2 symmetry is adopted to settle the conformation of **1**–**12** in the ground and the excited states. As shown in Fig. 2, Ir atom stays on the origin of the coordination system, the *z* axis coinciding with the C_2 symmetrical axis orients through Ir and the central C' atom in the acac cycle, *x* and *y* axes deviate 45° from the acac plane respectively. Three ligands are almost perpendicular to each other. DFT with Becke's three parameter functional and the Lee-Yang-Parr functional [43] (B3LYP) and the configuration interaction with single-excitation [44–46] (CIS) methods have been employed to optimize the geometry structures of the complexes in the ground and excited states, respectively. On the basis of the optimized geometry structures in the ground and excited states, the absorption and emission spectra in CH_2Cl_2 media were calculated by time-dependent DFT (TDDFT) [47–49] associated with the polarized continuum model (PCM) [50, 51]. This kind of theoretical approach (CIS/TDDFT) has been proven to be reliable for excited state investigations of transition-metal complexes [17,52–54].

In the calculations, the quasi-relativistic pseudo-potentials of Ir atom proposed by Hay and Wadt [55,56] with 17 valence electrons were employed, and LANL2DZ basis sets associated with the pseudo-potential were adopted. The basis sets were described as Ir (8s6p3d)/[3s3p2d], C and N (10s5p)/[3s2p], and H (4s)/[2s]. All of the calculations were accomplished by using the Gaussian 03 software package [57] on an Origin/3900 server.

To confirm the reproducibility of our calculation, we re-optimized the excited state of **1** with unrestricted non-hybrid DFT method with a hybrid Hartree-Fock/density functional model approach based on the Perdew–Burke–Erzenrhof (PBE) functional [58–60], referred to as PBE0 with SDD [61–64] basis set, and the phosphorescence in CH_2Cl_2 media of **1** was calculated by TDDFT method with PCM. The calculated results showed that the phosphorescence of **1** (508 nm) is nearly the same as result obtained by CIS/TDDFT methods with LANL2DZ basis set (505 nm).

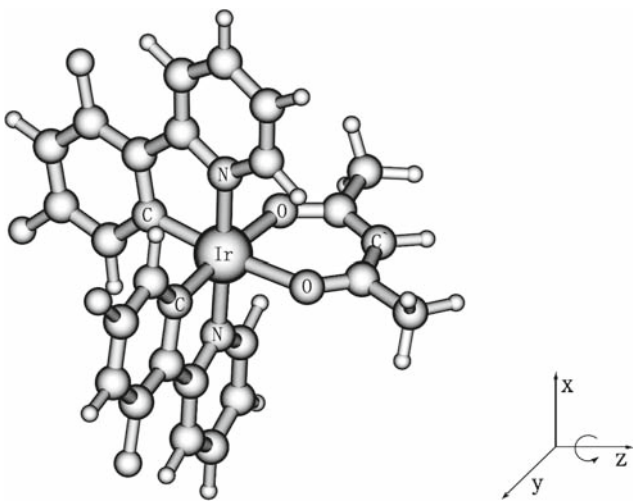

Fig. 2 The optimized geometry structures of **3** at B3LYP/LANL2DZ level

3 Results and discussion

3.1 The ground state geometries and the Frontier molecular orbital properties

The main optimized geometry parameters of **1**–**5** together with the available X-ray crystal diffraction data of **1** [1] are given in Table 1 and those of **6**–**12** are available in Supplementary Information (Table S1). Table 1 and Table S1 show that the optimized geometries of **1**–**12** are very similar in despite of different number and sites of the fluoro substituents on C^N ligands. For complex **1**, the calculated bond lengths of Ir–N (2.054 Å), Ir–C (2.009 Å), and Ir–O (2.192 Å) are overestimated by 0.01–0.04 Å compared with the measured values, while the calculated bond angles are close to the experimental values except that the O–Ir–O bond angle (85.4°) deviates slightly (4.6°) from the experimental value. Moreover, Fig. 2 shows that the three ligands are almost perpendicular to each other because C–N–Ir–O and C–N–Ir–C dihedral angles are close to 90°. The discrepancies of the geometry parameters between the calculated and measured values are reasonable and acceptable, since the real molecules are in tight crystal lattice, while the calculated molecules are free. The calculated results also showed that the bond lengths Ir–N (2.055 Å), Ir–C (2.005 Å), and Ir–O (2.176 Å) of **3** are comparable to the early corresponding theoretical results Ir–N (2.062 Å), Ir–C (2.002 Å), and Ir–O (2.190 Å) calculated at B3LYP (LANL2DZ for Ir and 6–31G(d) for other atoms) level [65].

Density functional theory calculation results indicated that all of the complexes have similar FMOs, the highest occupied molecular orbital (HOMO) is composed of d(Ir) and π(C^N), while the lowest unoccupied molecular orbital (LUMO) has predominant π^*(C^N) characters (see Tables 4, 5, S3–S12). Take **1** for example, the HOMO is composed of 50.0% d(Ir),

Table 1 The main optimized geometry structural parameters of complexes **1**–**5** in the ground and the triplet excited state at the B3LYP/LANL2DZ and CIS/LANL2DZ Level respectively, together with the experimental values of **1** and theoretical values of **3**

Parameters	1		2		3		4		5		1	3
	X^1A	A^3B	X^1A	A^3A	X^1A	A^3A	X^1A	A^3A	A^3A	X^1A	Exptl.[a]	Cal.[b]
Bond length (Å)												
Ir–N	2.054	2.084	2.053	2.085	2.055	2.082	2.057	2.082	2.056	2.082	2.011	2.062
Ir–C	2.009	2.035	2.010	2.034	2.005	2.032	2.015	2.044	2.016	2.044	2.004	2.002
Ir–O	2.192	2.182	2.186	2.169	2.176	2.162	2.160	2.145	2.156	2.141	2.147	2.190
Bond angle (deg)												
N–Ir–N	177.1	176.6	176.9	176.3	177.1	176.6	179.7	179.1	179.6	179.1	176.3	
O–Ir–O	85.4	82.5	85.7	83.0	86.0	83.3	86.8	84.0	87.1	84.3	90.0	
C–Ir–C	92.7	91.8	93.2	91.7	93.1	91.8	93.6	92.4	93.8	92.6		
Dihedral angle (deg)												
C–N–Ir–O	90.4	90.4	86.8	90.2	86.4	89.4	88.2	88.4	84.1	88.0		
C–N–Ir–C	85.4	87.2	84.8	87.0	84.8	86.7	84.3	85.1	83.5	84.8		

[a] From ref. [1]
[b] From ref. [65]

35.6% π (phenyl), and 7.1% π (pyridyl), while the LUMO has 27.1% π^* (phenyl) and 67.8% π^* (pyridyl), but the electron density of HOMO and LUMO are hardly contributed by fluoro substituents.

However, compared **2**–**12** with **1**, there is hardly influence to the HOMO and LUMO nature by adding fluoro on C^N ligands except that the energy levels are dramatically affected. Table 2 and Fig. 3 show the energy levels of HOMO and LUMO of all the complexes. We can see that: (1) Fluoro on phenyl ring leads to the decrease of the energy levels of the HOMO and LUMO, because the fluoro can withdraw electrons from the mainframe of the molecule. However, the decreasing tendency of the energy level of HOMO is more significant than that of LUMO, so the HOMO–LUMO (H–L) energy gap is expanded. (2) The fluoro on pyridyl ring also results in the decline of the HOMO and LUMO energy levels, but the decreasing tendency of the energy level of HOMO is less significant than that of LUMO, thus the H–L energy gap is narrowed. (3) By comparing **4** with **5**, we note that adding one more fluoro on site 3 of phenyl group in **5** decreases the

Table 2 The energy levels (eV) of HOMO and LUMO obtained by B3LYP/LANL2DZ method for the ground state

	1	2	3	4	5	6
LUMO	−1.568	−1.735	−1.961	−1.996	−2.193	−1.647
HOMO	−5.078	−5.282	−5.617	−5.874	−6.013	−5.323
H–L	3.510	3.547	3.656	3.878	3.820	3.676
	7	8	9	10	11	12
LUMO	−1.794	−1.773	−1.844	−1.886	−1.802	−1.897
HOMO	−5.265	−5.371	−5.033	−5.175	−5.198	−5.119
H–L	3.471	3.598	3.189	3.289	3.396	3.222

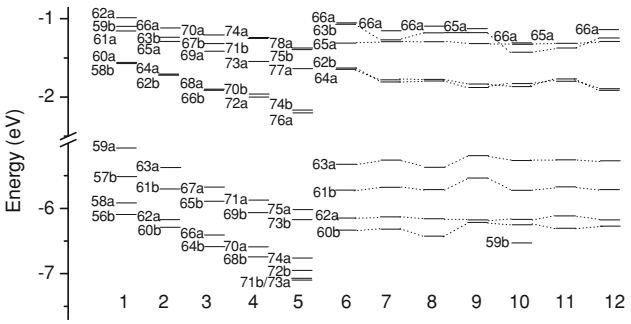

Fig. 3 The energy levels of important orbitals of **1**–**12**

H–L energy gap because fluoro on site 3 can more dramatically affect the energy level of LUMO than on other sites. Similarly, the comparison of **1** with **7** suggests adding a fluoro on site 3 of phenyl group decreases the H–L energy gap with the same reason. Moreover, we note that the energy level of LUMO for **7** is lower while that of HOMO is higher than those of **6** respectively. Similar variation trends have been obtained by Sun et al. [5] for [(5′-fpiq)$_2$Ir(acac)] and [(3′-fpiq)$_2$Ir(acac)] complexes, where the energy levels of HOMO are −4.85 and −4.89 eV and those of LUMO are −2.00 and −1.78 eV, respectively.

4 Absorptions in the CH_2Cl_2 media

The calculated absorptions of **1**, **2**, **5**, **6**, and **9** associated with their oscillator strengths, the main configurations, and the assignments are given in Table 3 and the FMO compositions of **2**, **5**, and **6** are summarized in Tables 4, 5, and S6, while those of other complexes are shown in Tables S2–S12. The fitted Gaussian type absorption curves with the

Table 3 The calculated absorptions of **1**, **2**, **5**, **6**, and **9** with TDDFT method

	Transition	Config. (CI coeff)	*E*/nm (eV)	Oscillator	Assignt.
1	$X^1A \rightarrow A^1B$	59a → 58b (0.68441)	453 (2.74)	0.0506	MLCTILCT
	$X^1A \rightarrow B^1B$	57b → 60a (0.67497)	391 (3.17)	0.0485	MLCT/LLCT
	$X^1A \rightarrow C^1B$	58a → 58b (0.59614)	352 (3.52)	0.1008	MLCT
	$X^1A \rightarrow D^1B$	56b → 62a (0.50162)	268 (4.63)	0.3884	ILCT
2	$X^1A \rightarrow A^1B$	63a → 62b (0.68269)	429 (2.89)	0.0521	MLCT/ILCT
	$X^1A \rightarrow B^1B$	61b → 64a (0.68174)	385 (3.22)	0.0530	MLCT/LLCT
	$X^1A \rightarrow C^1B$	62a → 62b (0.57196)	343 (3.61)	0.0884	MLCT
	$X^1A \rightarrow D^1B$	60b → 66a (0.49493)	263 (4.72)	0.3043	ILCT
5	$X^1A \rightarrow A^1B$	75a → 74b (0.68315)	403 (3.08)	0.0456	MLCT/ILCT
	$X^1A \rightarrow B^1B$	73b → 76a (0.68651)	381 (3.26)	0.0633	MLCT/LLCT
	$X^1A \rightarrow C^1B$	74a → 74b (0.67591)	331 (3.75)	0.0691	MLCT/ILCT
	$X^1A \rightarrow D^1B$	73a → 74b (0.58115)	282 (4.40)	0.1269	ILCT
	$X^1A \rightarrow E^1B$	72b → 78a (0.41232)	246 (5.03)	0.4343	ILCT
6	$X^1A \rightarrow A^1B$	63a → 62b (0.68761)	426 (2.91)	0.0473	MLCT/LLCT
	$X^1A \rightarrow B^1B$	61b → 64a (0.68411)	376 (3.30)	0.0597	MLCT/ILCT
	$X^1A \rightarrow C^1B$	61b → 65a (0.54623)	341 (3.63)	0.0498	MLCT/ILCT
	$X^1A \rightarrow D^1B$	60b → 66a (0.33015)	260 (4.77)	0.1142	ILCT
9	$X^1A \rightarrow A^1B$	63b → 62b (0.68686)	482 (2.57)	0.0659	MLCT/ILCT
	$X^1A \rightarrow B^1B$	61b → 64a (0.68997)	418 (2.97)	0.0354	MLCT/LLCT
	$X^1A \rightarrow C^1B$	62a → 62b (0.67104)	353 (3.51)	0.0731	MLCT
	$X^1A \rightarrow D^1B$	60b → 65a (0.42580)	269 (4.61)	0.3101	ILCT

Table 4 Molecular orbital compositions (%) in the ground state of **2** at B3LYP/LANL2DZ Level

Orbital	Energy (eV)	MO composition			Main bond nature	Ir components
		Ir	C^N	acac		
66a	−1.120	1.6	97.9	0.5	π^*(C^N)	
63b	−1.243	1.9	97.3	0.8	π^*(C^N)	
65a	−1.286	4.1	14.3	81.6	π^*(acac)	
64a	−1.710	3.7	93.5	2.8	π^*(C^N)	
62b	−1.718	3.3	95.3	1.4	π^*(C^N)	
HOMO–LUMO energy gap						
63a	−5.381	49.4	42.7	7.9	d(Ir)+π(C^N)	34.7 d_z^2, 13.5 d_{xy}
61b	−5.700	43.3	14.2	42.5	d(Ir)+π(C^N)+π(acac)	28.5 d_{xz}, 14.2 d_{yz}
62a	−6.176	66.2	27.3	6.5	d(Ir)+π(C^N)	63.1 $d_{x^2-y^2}$
60b	−6.294	0.6	93.5	5.9	π(C^N)	

calculated absorption data of **1**, **2**, **5**, **6**, and **9** are shown in Fig. 4 and those of other complexes are shown in Fig. S1. In order to intuitively understand the absorption transitions, the electronic density diagrams of **2** are displayed in Fig. 5 as an example, in which four single electron excitations corresponding to the maximal CI coefficients are involved.

From above tables and figs, we find the absorptions of **1**–**12** have similar absorption spectra and transition characters in despite of the fluoro substituent on the C^N ligands with different number and sites. Take **2** for example, Table 3 shows that there are four distinguishable absorption bands between 250 and 450 nm. The excitation of MO 63a → MO 62b contributes to the lowest-lying absorption at 429 nm. Table 4 shows that MO 63a (HOMO) is composed of 34.7% d_z^2(Ir), 13.5% d_{xy}(Ir), and 42.7% π(C^N), while MO 62b (LUMO) is π^*(C^N) type orbital. Therefore, this absorption band can be assigned to the combination of MLCT and ILCT transitions $\{[d_z^2(\mathrm{Ir}) + d_{xy}(\mathrm{Ir}) + \pi(\mathrm{C^\wedge N})] \rightarrow [\pi^*(\mathrm{C^\wedge N})]\}$. In the meanwhile, the lowest-lying absorption bands at 453, 418, 397, 403, 456, and 440 nm for **1**, **3**–**5**, **7**, and **8** have

Table 5 Molecular orbital compositions (%) in the ground state of **5** at B3LYP/LANL2DZ level

Orbital	Energy (eV)	MO composition			Main bond nature	Ir components
		Ir	C^N	acac		
78a	−1.387	1.4	98.2	0.4	π^*(C^N)	
75b	−1.392	1.4	97.9	0.7	π^*(C^N)	
77a	−1.640	3.3	13.7	83.0	π^*(acac)	
74b	−2.157	3.2	95.7	1.1	π^*(C^N)	
76a	−2.193	2.9	95.4	1.7	π^*(C^N)	
HOMO–LUMO energy gap						
75a	−6.013	47.5	44.0	8.5	d(Ir)+π(C^N)	32.5 d_z^2, 14.4 d_{xy}
73b	−6.177	32.8	16.8	50.4	d(Ir)+π(C^N)+π(acac)	21.6 d_{xz}, 6.4 d_{yz}
74a	−6.752	61.6	31.4	7.0	d(Ir)+π(C^N)	51.4 $d_{x^2-y^2}$
72b	−6.946	8.2	82.8	9.0	π(C^N)	
71b	−7.066	18.5	50.3	31.2	π(C^N)+pi(acac)	
73a	−7.095	7.8	91.0	1.2	π(C^N)	

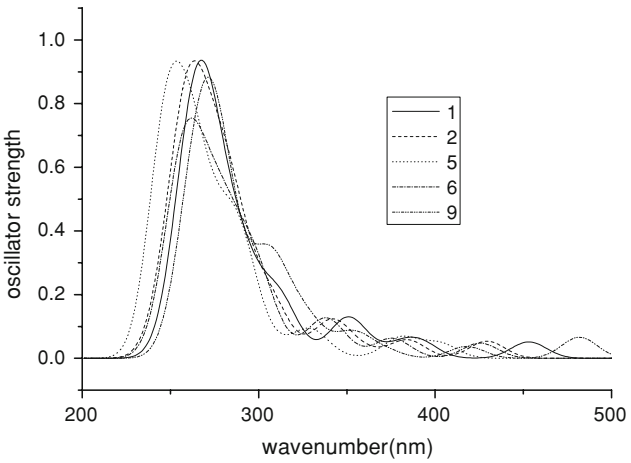

Fig. 4 The fitted Gaussian nature absorption curves of complexes **1**, **2**, **5**, **6**, and **9** at B3LYP/LANL2DZ level

the similar transition characters to that at 429 nm of **2** (see Tables 3, S2) which is consistent with the measured values 497 nm for **1**, 390 nm for **4**, and 395 nm for **5** [4,35]. But for **6** and **9**–**12**, the lowest-lying absorptions show some different characteristic. Take complex **6** for example, Table S6 shows that MO 63a has 35.0% d_z^2(Ir), 11.5% $d_{x^2-y^2}$(Ir), and 42.4% π(C^N), while 62b is dominantly composed of $\pi*$(C^N). Thus the lowest-lying absorption at 426 nm of **6** can be described as {[d_z^2(Ir) + $d_{x^2-y^2}$(Ir) + π(C^N)] → [π^*(C^N)]} transition with MLCT/ILCT characters, and the lowest-lying absorption bands at 482, 482, 459, and 477 nm of **9**–**12** have the similar transition characters to that at 426 nm of **6**. To conclude, the above lowest-lying absorptions of **1**–**12** can be attributed to {[d(Ir) + π(C^N)] → [π^*(C^N)]} transition with the MLCT/ILCT character.

Another calculated differential absorption at 385 nm of **2** is assigned to {[d_{xz}(Ir) + d_{yz}(Ir) + π(acac)] → [π^*(C^N)]} transition with MLCT/LLCT character (see Table 4). The

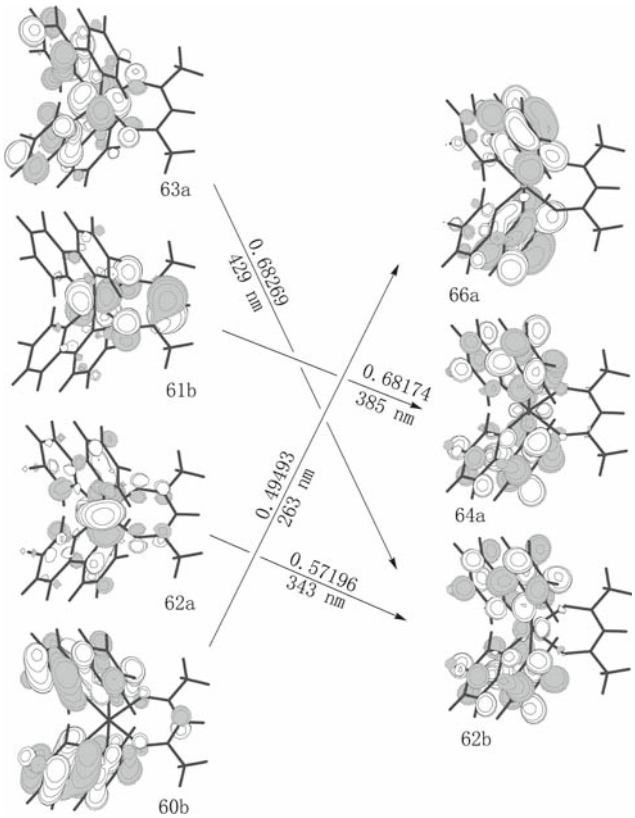

Fig. 5 Single electron transitions with the maximum CI coefficients under TD–DFT calculations for the 429, 385, 343 and 263 nm absorptions of complex **2** at B3LYP/LANL2DZ level

absorption at 343 nm of **2** is also attributed to MLCT but with different d(Ir) composition as shown in Table 4 that MO 62a has 63.1% $d_{x^2-y^2}$(Ir) and 27.3% π(C^N), so this absorption can be described as {[$d_{x^2-y^2}$(Ir)+π(C^N)] → [π^*(C^N)]} transition. The $X^1A \rightarrow B^1B$ and $X^1A \rightarrow C^1B$ absorptions of **1** (391 and 352 nm), **4** (374 and 330 nm), **5** (381 and 331 nm), **7** (397 and 354 nm), and **8** (391 and 348 nm) have the

similar transition characters to those at 385 and 343 nm of **2**, respectively (see Table S2). The absorption at 338 nm of **3** can be assigned to the combination of MLCT and ILCT transitions $\{[d_z^2(\mathrm{Ir}) + d_{xy}(\mathrm{Ir}) + \pi(\mathrm{C^\wedge N})] \rightarrow [\pi^*(\mathrm{C^\wedge N})]\}$ (Table S2). And the absorption at 341 nm of **6** is attributed to $\{[d_{xz}(\mathrm{Ir}) + d_{yz}(\mathrm{Ir}) + \pi(\mathrm{acac})] \rightarrow [\pi^*(\mathrm{C^\wedge N})]\}$ transition with MLCT/LLCT character (see Table 3). The calculated results also showed that the $X^1A \rightarrow B^1B$ absorption of **9** is assigned to $\{[d_{yz}(\mathrm{Ir}) + \pi(\mathrm{C^\wedge N})] \rightarrow [\pi^*(\mathrm{C^\wedge N})]\}$ transition, and the $X^1A \rightarrow C^1B$ absorption can be described as $\{[d_{x^2-y^2}(\mathrm{Ir}) + d_{xy}(\mathrm{Ir}) + \pi(\mathrm{C^\wedge N})] \rightarrow [\pi^*(\mathrm{C^\wedge N})]\}$ transition (see Table S2).

In the high energy region, the absorption bands of **1**–**12** are at 240–270 nm, and they have similar transition character. Take complex **2** for example, both of MOs 66a and 60b generally concentrate on C^N ligand, thus the high-energy absorption at 263 nm of **2** is attributed to $\{[\pi(\mathrm{C^\wedge N})] \rightarrow [\pi^*(\mathrm{C^\wedge N})]\}$ transition with ILCT transition character and the high-energy absorption of **2**–**12** have the similar ILCT transition character.

On experiment, the absorption bands at 253 and 303 nm of **4** and 248 and 288 nm of **5** both are all concluded to $^1(\pi \rightarrow \pi^*)$ transition because there is no distinguishable feature of the spectra [35]. Herein, the calculated absorptions at 249 and 297 nm of **4**, 246 and 282 nm of **5** are attributed to the above experimental values. Specially, we can distinguish the two absorption bands theoretically according to the transition nature. Take **5** for example, although both of the absorptions can be described as $\{[\pi(\mathrm{C^\wedge N})] \rightarrow [\pi^*(\mathrm{C^\wedge N})]\}$ transition, they exhibit slight quantitative difference. The excitation of MO 73a → MO 74b is responsible for the absorption at 282 nm of **5** (see Table 3). Table 5 shows that MO 73a has 31.3% π(pyridyl) and 52.8% π(phenyl), while MO 74b has 43.5% π^*(pyridyl) and 37.6% π(phenyl). Therefore, this absorption band can be assigned to ILCT $\{[\pi(\mathrm{C^\wedge N})] \rightarrow [\pi^*(\mathrm{C^\wedge N})]\}$ containing ca. 10% $\{[\pi(\mathrm{phenyl})] \rightarrow [\pi^*(\mathrm{pyridyl})]\}$ transition. With respect to the absorption at 246 nm of **5**, the excitation of MO 72b → MO 78a has the largest CI coefficient and is in charge of the absorption. MO 72b has 33.8% π(pyridyl) and 44.1% π(phenyl), MO 78a is composed of 65.2% π^*(pyridyl) and 16.0% π^*(phenyl). Therefore, this absorption band can be assigned to ILCT transition with ca. 30% $\{[\pi(\mathrm{phenyl})] \rightarrow [\pi^*(\mathrm{pyridyl})]\}$ transition. In the meanwhile, the high energy absorptions at 249 and 297 nm of **4** have the similar transition paths to those at 246 and 282 nm of **5**, respectively (see Table S5).

Experimentally, the absorption bands between 250 and 350 nm of $(\mathrm{C^\wedge N})_2\mathrm{IrL}$ (C^N = ppy, tpy, bzq, and ppz etc. L = acac, tmd, and bza etc.) were assigned to dipole-allowed $^1[\pi \rightarrow \pi^*]$ transition within C^N ligands, while those above 400 nm were described as ^{1}MLCT transition between Ir and C^N ligands [1,35]. Obviously, our calculation results are well consistent with the experimental conclusions. Furthermore, our calculations reveal the transition nature in detail.

The calculation results showed that the lowest-lying absorptions of **1**–**5** are blue-shifted with the increasing number of the fluoro on phenyl group because of the broader H–L energy gaps. The different substituent sites of fluoro on phenyl groups have the different influence to the absorption because the fluoro on different site can stabilize the HOMO with different extent. The fluoro resides on sites 1, 2, and 4 can lead to a blue-shift compared to that on site 3. Furthermore, the lowest-lying absorptions are somewhat red-shifted when the fluoros are on the pyridyl group. This is because the fluoro on pyridyl can more significantly lower the energy level of LUMO than that of HOMO resulting in the decrease of H–L energy gap, which is consistent with the FMO properties.

4.1 The geometry structures in the triplet excited state and the emissions in the CH_2Cl_2 media

The main geometry structural parameters of the complexes in the A^3A (**2**–**5**, **7**, **9**, and **11**) and A^3B (**1**, **6**, **8**, **10**, and **12**) excited states optimized by CIS method are given in Tables 1 and S1. In the lowest-lying triplet excited state, almost no variation of the geometry structures of **1**–**12** can be found relative to those in the ground state except that the Ir–N, Ir–C, and Ir–O bond lengths change slightly and with the similar variation trends for all these complexes. The calculated Ir–C and Ir–N bond lengths in excited state relax by about 0.03 Å, but the Ir–O bond length is strengthened by ca. 0.01–0.02 Å. The calculated O(1)–Ir–O(2) bond angle reduces by 2.0°–3.0°, while the C(3)–N(2)–Ir–O(1) and C(3)–N(2)–Ir–C(1) dihedral angles change less than 4.0°. The slight difference of the geometry structures result from the electron transition from Ir–C^N bonding orbital to π^*(C^N) orbital (vide infra) upon excitation.

The calculated phosphorescence of **1**–**12** in CH_2Cl_2 media and the measured emissions are given in Table 6; the FMO compositions responsible for the emissions are summarized in Tables 7 and S13.

The calculated phosphorescence at 505 nm (2.46 eV), 452 nm (2.74 eV), and 461 nm (2.69 eV) of **1**, **4**, and **5** agree well with their, respectively, experimental results at 516 nm [4] (2.40 eV), 465 nm [35] (2.67 eV), and 479 nm [35] (2.59 eV). In regard to **5**, the excitation of MO 75a → MO 76a with the configuration coefficient of 0.59541 is responsible for the emission at 461 nm (see Table 6). Table 7 shows that MO 75a has 33.2% d_z^2(Ir), 14.5% d_{xy}(Ir), and 40.8% π(C^N), while MO 76a is π^*(C^N) type orbital. Thus the emission at 461 nm originates from $^3\{[d_z^2(\mathrm{Ir}) + d_{xy}(\mathrm{Ir}) + \pi(\mathrm{C^\wedge N})][\pi^*(\mathrm{C^\wedge N})]\}$ excited state with ^{3}MLCT/^{3}ILCT characters. Experimentally, the measured phosphorescence

Table 6 The calculated phosphorescent emissions in CH_2Cl_2 media of **1**–**12** with TDDFT method, together with the corresponding experimental values

	Transition	Config. (CI coeff)	*E*/nm (eV)	Assignt.	$\lambda_{exptl.}$ (nm)
1	$A^3B \rightarrow X^1A$	59a → 58b (0.66853)	505 (2.46)	MLCT/ILCT	516 (2.40)[a]
2	$A^3A \rightarrow X^1A$	63a → 64a (0.61073)	475 (2.61)	MLCT/ILCT	
3	$A^3A \rightarrow X^1A$	67a → 68a (0.60292)	462 (2.68)	MLCT/ILCT	
4	$A^3A \rightarrow X^1A$	71a → 72a (0.54937)	452 (2.74)	MLCT/ILCT	465 (2.67)[b]
5	$A^3A \rightarrow X^1A$	75a → 76a (0.59541)	461 (2.69)	MLCT/ILCT	479 (2.59)[b]
6	$A^3B \rightarrow X^1A$	63a → 62b (0.63219)	482 (2.57)	MLCT/ILCT	
7	$A^3A \rightarrow X^1A$	63a → 64a (0.67314)	511 (2.43)	MLCT/ILCT	
8	$A^3B \rightarrow X^1A$	63a → 62b (0.66445)	488 (2.54)	MLCT/ILCT	
9	$A^3A \rightarrow X^1A$	63a → 64a (0.67867)	521 (2.38)	MLCT/ILCT	
10	$A^3B \rightarrow X^1A$	63a → 62b (0.67282)	514 (2.41)	MLCT/ILCT	
11	$A^3B \rightarrow X^1A$	63a → 64a (0.67276)	500 (2.48)	MLCT/ILCT	
12	$A^3A \rightarrow X^1A$	63a → 62b (0.68339)	528 (2.35)	MLCT/ILCT	

[a] From ref. [4]
[b] From ref. [35]

Table 7 Molecular orbital compositions (%) in the A^3A excited states of **5** at B3LYP/LANL2DZ level

Orbital	Energy (eV)	MO composition			Main bond nature	Ir components
		Ir	(C^N)	acac		
76a	−2.143	3.0	95.9	1.1	π^*(C^N)	
74b	−2.144	2.5	96.4	1.1	π^*(C^N)	
HOMO–LUMO energy gap						
75a	−5.919	48.5	40.8	10.6	d(Ir)+π(C^N)	33.2 d_z^2, 14.5 d_{xy}

of **5** at 479 nm in CH_2Cl_2 media has been tentatively assigned to ^{3}MLCT emission [35].

Tables 6 and S13 show that the natures of the phosphorescence at 475, 462, 452, 511, and 488 nm for **2**–**4**, **7**, and **8**, respectively, are similar to that at 461 nm of **5**, they all originate from ^{3}MLCT/^{3}ILCT^3{[d_z^2(Ir)+d_{xy}(Ir)+π(C^N)][π^*(C^N)]} excited state. But the phosphorescence at 505, 482, 521, 514, 500, and 528 nm of **1**, **6**, and **9**–**12**, respectively, originate from ^{3}{[d_z^2(Ir)+$d_{x^2-y^2}$(Ir)+π(C^N)][π^*(C^N)]} excited state with different d(Ir) component. The calculated absorption results revealed that the lowest-lying absorption of **1**–**12** are dominantly assigned to the combination of MLCT and ILCT electronic transition, while the emission is just the reverse processes of the corresponding lowest-lying absorption because of the same transition character and symmetry. The energy differences between the calculated lowest-lying absorptions and the emissions are 0.28, 0.27, 0.28, 0.39, 0.39, 0.34, 0.29, 0.28, 0.19, 0.23, 0.22, and 0.25 eV for **1**–**12**, respectively. To intuitively understand the emission transition of the complexes, we display the electron density diagrams of the emission at 475 nm for **2** in Fig. 6 as an example.

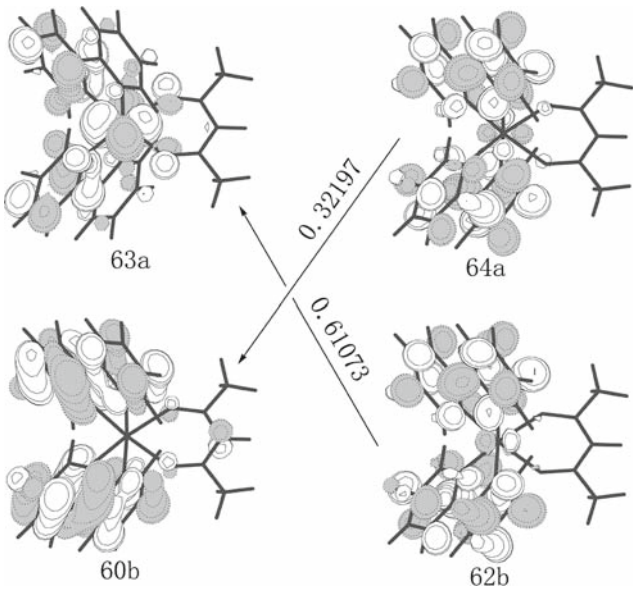

Fig. 6 Single electron transition with |CI coefficients| > 0.1 under TD–DFT calculation for the 475 nm emission of complex **2**

Although the fluoro substituents cannot change the transition character of the emission, the emission color can be adjusted by the fluoro number and the site to stay on. Figure 7 shows the calculated transition energy of phosphorescence in CH_2Cl_2 media of **1**–**12** to compare the variation of phosphorescence by adding fluoro with different number and sites. Table 6 and Fig. 7 show that among **1**–**4**, the emissions are blue-shifted (0.15–0.28 eV) with increasing the number of the fluoro on phenyl group because more fluoro can make the H–L energy gap broader. On shifting the fluoro among sites 1, 2, and 4, the emissions of them vary within

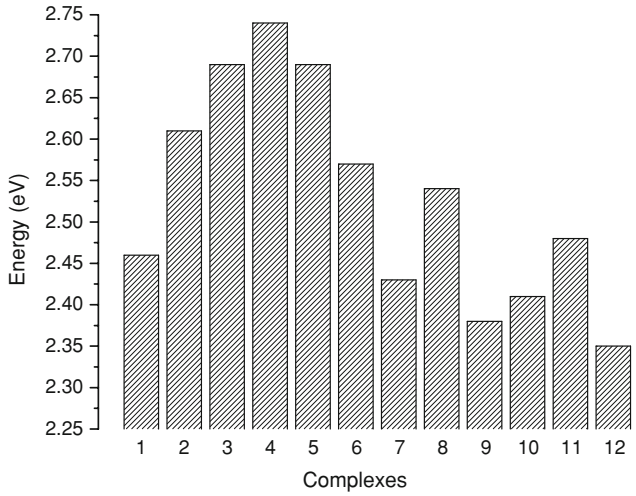

Fig. 7 The calculated phosphorescent energy in CH_2Cl_2 media of **1**–**12** under TD–DFT calculation

0.07 eV to high energy area. With respect to **7**, the emission is red-shifted about 0.03 eV by adding a fluoro on site 3 in comparison with **1**. In addition, adding a fluoro on site 3 in complex **5** also results in minor red-shift ca. 0.05 eV compared with complex **4**. On experiment, Naso and co-workers [35] similarly observed that the reduction potential values of $(F_4ppy)Ir(acac)$ **5** were less negative than $(F_3ppy)Ir(acac)$ **4**. All these facts indicated that attaching a fluoro on site 3 of phenyl group can slightly narrow the H–L gap. For the case of pyridyl group, adding a fluoro on sites 5, 6, and 8 in **9**, **10**, and **12** results in a small red-shift (below 0.1 eV), but the fluoro on site 7 results in somewhat blue-shift related to **1**. So we can see the phenyl groups are more significant than pyridyl fragments in adjusting the emission properties.

5 Conclusion

The present work theoretically investigated the geometry structures, absorptions, and phosphorescence properties of a series of Iridium(III) cyclometallated complexes with fluoro substitutents on the C^N ligands, and the following conclusions can be drawn.

(1) Complexes **1**–**12** have the similar geometry structures in both the ground and excited states. The energy levels of the FMOs are influenced by varying either the sites or the numbers of the fluoro on the phenyl groups but hardly affected by the substituents situated on the pyridyl fragments.

(2) The lowest-lying absorptions of the complexes can be described as $[d(Ir) + \pi(C^{\wedge}N)] \rightarrow [\pi^*(C^{\wedge}N)]$ MLCT/ILCT transitions, while the emissions of them originate from $^3\{[d(Ir) + \pi(C^{\wedge}N)][\pi^*(C^{\wedge}N)]\}$ excited states. When the electron-withdrawing fluoros are introduced into the phenyl groups, the lowest-lying absorption and the emission are usually blue-shifted. As an exception, the fluoro on site 3 of phenyl can lead to a slight red-shift.

(3) When the electron-withdrawing fluoros located on the pyridyl fragment, the lowest-lying absorptions and emission are somewhat red-shifted but the fluoro on site 7 can lead to a minor blue-shift.

The above discussions reveal that the photophysical properties of the cyclometalated iridium complexes can be finely tuned by systematic control of the number and the site of the substituents on the phenyl ring.

Acknowledgments This work was supported by the Natural Science Foundation of China (Grant Nos. 20173021, 20333050, 20573042, and 2070315).

References

1. Lamansky S, Djurovich P, Murphy D, Abdel-Razzaq F, Kwong R, Tsyba I, et al (2001) Inorg Chem 40:1704. Medline. doi:10.1021/ic0008969
2. Sajoto T, Djurovich PI, Tamayo A, Yousufuddin M, Bau R, Thompson ME (2005). Inorg Chem 44:7992. Medline. doi:10.1021/ic051296i
3. Lamansky S, Djurovich P, Murphy D, Abdel-Razzaq F, Lee HE, Adachi C, et al (2001) J Am Chem Soc 123:4304. Medline. doi:10.1021/ja003693s
4. Colombo MG, Gudel HU (2001) Inorg Chem 32:3081. doi:10.1021/ic00066a019
5. Yang CH, Su WL, Fang KH, Wang SP, Sun IW (2006) Organometallics 25:4514. doi:10.1021/om060323p
6. Stampor W, Mežyk J, Kalinowski J (2004) Chem Phys 300:189. doi:10.1016/j.chemphys.2004.01.023
7. Stampor W, Mežyk J (2007) Chem Phys 337:151. doi:10.1016/j.chemphys.2007.07.016
8. Deng YJ, Huang MJ (2006) Chem Phys 321:133. doi:10.1016/j.chemphys.2005.08.009
9. Jansson E, Minaev B, Schrader S, Ågren H (2007) Chem Phys 333:157. doi:10.1016/j.chemphys.2007.01.021
10. King KA, Spellane PJ, Watts RJ (1985) J Am Chem Soc 107:1431. doi:10.1021/ja00291a064
11. Hay PJ (2002) J Phys Chem A 106:1634. doi:10.1021/jp013949w
12. Yu SC, Kwok CC, Chan WK, Che CM (2003) Adv Mater 15:1643. doi:10.1002/adma.200305002
13. Che CM, Chan SC, Xiang HF, Chan MCW, Liu Y, Wang Y (2004) Chem Commun (Camb) 1484. Medline. doi:10.1039/b402318h
14. D'Andrade BW, Holmes RJ, Forrest SR (2004) Adv Mater 16:624. doi:10.1002/adma.200306670
15. Coppo P, Duati M, Kozhevnikov VN, Hofstraat JW, De Cola L (2004) Angew Chem Int Ed 43:2
16. Furuta PT, Deng L, Garon S, Thompson ME, Frechet JMJ (2004) J Am Chem Soc 126:15388. Medline. doi:10.1021/ja0446247
17. Sun M, Niu B, Zhang JP (2008) Theor Chem Acc. doi:10.1007/s00214-008-0410-2
18. Grem G, Leditzky G, Ulrich B, Leising G (1992) Adv Mater 4:36. doi:10.1002/adma.19920040107
19. Pei Q, Yang Y (1996) J Am Chem Soc 118:7416. doi:10.1021/ja9615233
20. Kido J, Hongawa K, Okuyama K, Nagai K (1993) Appl Phys Lett 63:2627. doi:10.1063/1.110402

21. Andersson MR, Berggren M, Inganäs O, Gustafsson G, Gustafsson-Carlberg JC, Selse D et al (1995) Macromolecules 28:7525. doi:10.1021/ma00126a033
22. Granstrom M, Inganas O (1996) Appl Phys Lett 68:147. doi:10.1063/1.116129
23. Andersson MR, Thomas O, Mammo W, Sevensson M, Theander M, Inganäs O (1999) J Mater Chem 9:1933. doi:10.1039/a902859e
24. Dedeian K, Shi JM, Shepherd N, Forsythe E, Morton DC (2005) Inorg Chem 44:4445 Medline. doi:10.1021/ic050324u
25. Ashenhurst J, Brancaleon L, Hassan A, Liu W, Schmider H, Wang S et al (1998) Organometallics 17:3186. doi:10.1021/om980199c
26. Ho KY, Yu WY, Cheung KK, Che CM (1999) Dalton Trans 1581
27. Wu Q, Lavigne JA, Tao Y, D'Iorio M, Wang S (2000) Inorg Chem 39:5248. Medline. doi:10.1021/ic000465q
28. Liu SF, Wu Q, Schmider HL, Aziz H, Hu NX, Popovic Z et al (2000) J Am Chem Soc 122:3671. doi:10.1021/ja9944249
29. Weber L, Domke I, Schmidt C, Braun T, Stammler HG, Neumann B (2006) Dalton Trans 2127. Medline. doi:10.1039/b514920g
30. Lee CM, Chin KF, Peng SM, Che CM (1993) Dalton Trans 467
31. Ma Y, Chao HY, Wu Y, Lee ST, Yu WY, Che CM (1998) Chem Commun (Camb) 2491. doi:10.1039/a805236k
32. Gao S, Wu Q, Wu G, Wang S (1998) Organometallics 17:4666. doi:10.1021/om980435j
33. Ashenhurst J, Wu G, Wang S (2000) J Am Chem Soc 122:2541. doi:10.1021/ja992868z
34. Tamayo AB, Garon S, Sajoto T, Djurovich PI, Tsyba IM, Bau R et al (2005) Inorg Chem 44:8723. Medline. doi:10.1021/ic050970t
35. Ragni R, Plummer EA, Brunner K, Hofstraat JW, Babudri F, Farinola GM et al (2006) J Mater Chem 16:1161. doi:10.1039/b512081k
36. Babudri F, Farinola GM, Naso F, Ragni R (2007) Chem Commun (Camb) 1003. Medline. doi:10.1039/b611336b
37. Di Censo D, Fantacci S, De Angelis F, Klein C, Evans N, Kalyanasundaram K, Bolink HJ, Gra1tzel M, Nazeeruddin MK (2008) Inorg Chem 47:980. Medline. doi:10.1021/ic701814h
38. De Angelis F, Fantacci S, Evans N, Klein C, Zakeeruddin SM, Moser JE, Kalyanasundaram K, Bolink HJ, Gra1tzel M, Nazeeruddin MK, (2007) Inorg Chem 46:5989. Medline. doi:10.1021/ic700435c
39. Kwon TH, Cho HS, Kim MK, Kim JW, Kim JJ, Lee KH et al (2005) Organometallics 24:1578. doi:10.1021/om049419e
40. Grushin VV, Herron N, LeCloux DD, Marshall WJ, Petrov VA, Wang Y (2001) Chem Commun (Camb) 1494. doi:10.1039/b103490c
41. Wang Y, Herron N, Grushin VV, LeCloux D, Petrov VA (2001) Appl Phys Lett 79:449. doi:10.1063/1.1384903
42. Runge E, Gross EKU (1984) Phys Rev Lett 52:997. doi:10.1103/PhysRevLett.52.997
43. Becke AD (1993) J Chem Phys 98:5648. doi:10.1063/1.464913
44. Stanton JF, Gauss J, Ishikawa N, Head-Gordon M (1995) J Chem Phys 103:4160. doi:10.1063/1.469601
45. Foreman JB, Head-Gordon M, Pople A (1992) J Phys Chem 96:135. doi:10.1021/j100180a030
46. Waiters VA, Hadad CM, Thiel Y, Colson SD, Wibergy KB, Johnson PM, et al (1991) J Am Chem Soc 113:4782. doi:10.1021/ja00013a011
47. Stratmann RE, Scuseria GE (1998) J Chem Phys 109:8218. doi:10.1063/1.477483
48. Matsuzawa NN, Ishitani A (2001) J Phys Chem A 105:4953. doi:10.1021/jp003937v
49. Casida ME, Jamorski C, Casida KC, Salahub DR (1998) J Chem Phys 108:4439. doi:10.1063/1.475855
50. Cossi M, Scalmani G, Regar N, Barone V (2002) J Chem Phys 117:43. doi:10.1063/1.1480445
51. Barone V, Cossi M (1997) J Chem Phys 107:3210. doi:10.1063/1.474671
52. Monat JE, Rodriguez JH, McCusker JK (2002) J Phys Chem A 106:7399. doi:10.1021/jp020927g
53. Liu T, Xia BH, Zhou X, Zhang HX, Pan QJ, Gao JS (2007) Organometallics 26:143. doi:10.1021/om0606338
54. Mennucci B, Cappelli C, Cammi R, Tomasi J (2007) Theor Chem Acc 117:1029. doi:10.1007/s00214-006-0221-2
55. Hay PJ, Wadt WR (1985) J Chem Phys 82:299. doi:10.1063/1.448975
56. Hay PJ, Wadt WR (1985) J Chem Phys 82:270. doi:10.1063/1.448799
57. Frisch MJ, Trucks GW, Schlegel HB, Scuseria GE, Robb MA, Cheeseman JR Jr Montgomery JA, Vreven T, Kudin KN, Burant JC, Millam JM, Iyengar SS, Tomasi J, Barone V, Mennucci B, Cossi M, Scalmani G, Rega N, Petersson GA, Nakatsuji H, Hada M, Ehara M, Toyota K, Fukuda R, Hasegawa J, Ishida M, Nakajima T, Honda Y, Kitao O, Nakai H, Klene M, Li X, Knox JE, Hratchian H P, Cross JB, Adamo C, Jaramillo J, Gomperts R, Stratmann RE, Yazyev O, Austin AJ, Cammi R, Pomelli C, Ochterski JW, Ayala PY, Morokuma K, Voth GA, Salvador P, Dannenberg JJ, Zakrzewski VG, Dapprich S, Daniels AD, Strain MC, Farkas O, Malick DK, Rabuck AD, Raghavachari K, Foresman JB, Ortiz JV, Cui Q, Baboul AG, Clifford S, Cioslowski J, Stefanov BB, Liu G, Liashenko A, Piskorz P, Komaromi I, Martin RL, Fox DJ, Keith T, Al-Laham MA, Peng CY, Nanayakkara A, Challacombe M, Gill P MW, Johnson, B Chen W, Wong MW, Gonzalez C, Pople JA (2004) Gaussian 03, Revision C02, Gaussian, Inc: Wallingford
58. Perdew JP, Burke K, Ernzerhof M (1996) Phys Rev Lett 77:3865 Medline. doi:10.1103/PhysRevLett.77.3865
59. Perdew JP, Burke K, Ernzerhof M (1997) Phys Rev Lett 78:1396. doi:10.1103/PhysRevLett.78.1396
60. Adamo C, Barone V (1999) J Chem Phys 110:6158. doi:10.1063/1.478522
61. Häussermann U, Dolg M, Stoll H, Preuss H, Schwerdtfeger P, Pitzer RM (1993) Mol Phys 78:1211. doi:10.1080/00268979300100801
62. Kuechle W, Dolg M, Stoll H, Preuss H (1994) J Chem Phys 100:7535. doi:10.1063/1.466847
63. Leininger T, Nicklass A, Stoll H, Dolg M, Schwerdtfeger P (1996) J Chem Phys 105:1052. doi:10.1063/1.471950
64. Andrae D, Haeussermann U, Dolg M, Stoll H, Preuss H (1990) Theor Chim Acta 77:123. doi:10.1007/BF01114537
65. Park NG, Choi GC, Lee YH, Kim YS (2006) Curr Appl Phys 6:620. doi:10.1016/j.cap.2005.04.007